Virtual CT test environment used to study the effect of individual influence factors

Crhistian R Baldo[1], Wim Dewulf[2]

[1] Center for Engineering, Modeling and Applied Social Sciences, CECS / UFABC, Brazil, crhistian.baldo@ufabc.edu.br

[2] Department of Mechanical Engineering, KU Leuven, Belgium, wim.dewulf@kuleuven.be

Abstract

Computed Tomography (CT) features a complex measurement chain and the measurement accuracy relies on selecting suitable scan parameters, which are very dependent on the measuring task. To develop a broader understanding of the effect of a given influence factor on the measurement of dimensional features, through a what-if analysis, the use of computer simulation has to be considered as a reasonable alternative to the analytical and experimental approaches. In this regard, this research focuses on the construction of a digital twin of a CT instrument designed for dimensional measurement using a commercial simulation tool and the utilization of the virtual measurement scene to increase the understanding of the relationships between input parameters and dimensional quantities of a mechanical test object. The main outcomes of the performed simulation-based sensitivity analysis and their correlation with some results obtained with the physical CT instrument are described as well.

Keywords: CT metrology, measurement accuracy, sensitivity analysis, simulation-based experiments.

1 Background

CT as an asset of dimensional metrology has shown unprecedented capability of sampling high point coordinate data density of intricate mechanical parts, including their structures that cannot be reached by conventional (tactile and optical) sensors, thus being a technology that can contribute tremendously to the current necessities of manufacturing metrology. The complexity of the CT measurement chain gives rise to a multitude of factors that influence the result of a measurement [1]; to a certain extent, the measurement accuracy depends on the choice of proper settings of the CT instrument, such as: (x-ray tube) voltage and current, (detector) integration time, image averaging and gain, (rotational stage) number of radiographs, (object) magnification and orientation, (image and data processing) segmentation, point extraction and fitting algorithm; which require a skilled CT metrologist who can make the proper tuning of all them. To assist the CT metrologist with the choice of proper parameters for a given measuring task, analytical simulation tools have been developed [2–5].

This way, coordinate metrology with CT can benefit from the overall concept of digital twins, i.e., virtual replicas of the actual physical device. In the digital environment, for example, the many variables under the control of the metrologist (or over which his/her has some degree of control) can be previously tuned (and tests undertaken), leaving a few adjustments to be performed thereafter on the physical CT instrument. Digital twins can be applied as well to investigate how the uncertainty of the result of a measurement can be apportioned among different influence quantities. In this regard, this paper first illustrates the creation of a digital twin of a CT measurement process on a commercial simulation program (please refer to section 2). The digital twin was subsequently used to isolate and quantify how some influence factors affect the result of dimensional measurements, which would be difficult (or even impossible) to do analytically or experimentally; the main experimental outcomes and the correlation with the results obtained on the physical twin are outlined in section 3. The concluding remarks are presented in section 4.

2 Virtual measurement design

In this research, the computer simulation program for quantitative description of radiographic testing - aRTist: analytical RT inspection simulation tool, version 2.10.0 64 bit, by the German Federal Institute of Materials Research and Testing (BAM) was chosen to develop a digital twin of a commercial CT instrument. The digital platform allows the CT metrologist to define realistic parameters for the x-ray tube, the detector and the test object, as well as to include some disturbing factors to be considered during simulation. To be loaded and included in the virtual scene of the simulation software, the mathematical model of the test object needs to be converted into a STL mesh, which was carried out within the software VG Studio MAX, version 3.3.2 64 bit, using the mesh accuracy preset called ‘extra high’. In the virtual measurement scene, the radiation intensity and spectrum in each detector pixel is calculated by attenuating the input spectrum along each ray from the source point, crossing the test object, to the corresponding pixel. The remaining of this section contains further information about the measurands, the creation of the CT measurement scene on the virtual platform, and the influence factors to be investigated.

2.1 Description of the test object

The test object considered in this research was a component that forms the drive system of a window lift mechanism, made of acetal photopolymer (ρ = 1.42 g/cm^3) and manufactured by injection molding. Figure 1 exhibits the physical quantities to be measured, i.e. the measurands, embracing intrinsic characteristics (size), situation characteristics (distance) and form tolerances

https://doi.org/10.58286/26577

(circularity, flatness), as follows: **cir-1** (outer diameter and form), **cir-2** (outer diameter and form), **cir-3** (outer diameter and form), **cir-4** (inner diameter), **cir-5** (inner diameter), **pln-1** (flatness for the whole surface and flatness on a unit basis), **pln-2** (flatness for the whole surface and flatness on a unit basis), **pln-3** (flatness for the whole surface), and distance between pln-1/pln-2, pln-1/pln-3, pln-2/pln-3. The general idea is to exploit the measurement process as much as possible; the variety of measurands was purposely chosen as they may respond distinctly to the variables associated with the CT measurement process. It is worthy of notice that the test object was previously measured on the physical CT instrument Carl Zeiss IMT METROTOM 1500 (of the Reference Center 'Metrology and Instrumentation' CMI, CERTI Foundation, Brazil) housed in a temperature-controlled laboratory kept at (20 ± 1) °C. This way, the real measurement setup and results obtained for some characteristics of the test object can be compared with the virtual results (obtained in this research). Please refer to Fernandes et al. [6] for more details on the analyses of the physical test object.

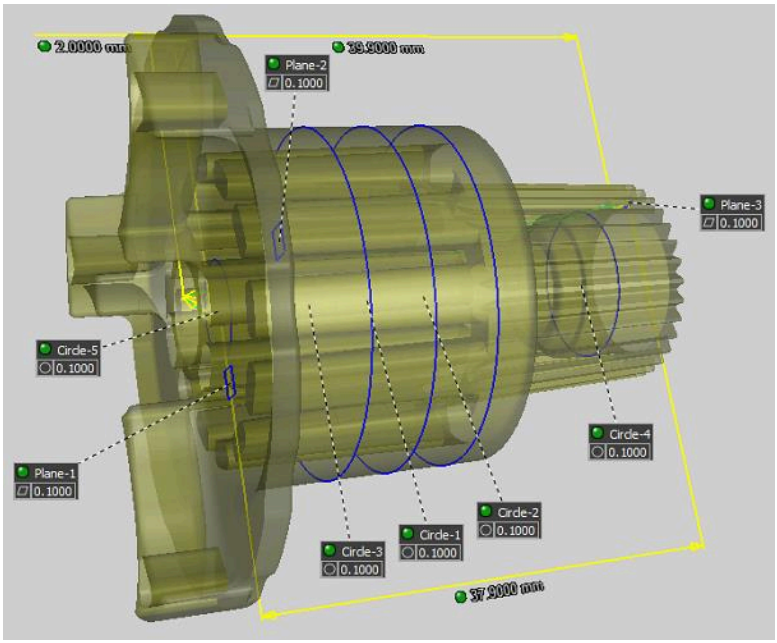

Figure 1: Ideal features of the test object to which the extracted points were associated; from the ideal features, the intrinsic characteristics (size), the situation characteristics (distance) and the form tolerances (circularity and flatness) were evaluated.

2.2 Preparation of the measurement scene

Based on data obtained from manufacturers' specifications, technical standards and empirical tests, the first generation of the CT system Carl Zeiss IMT METROTOM 1500 was modeled. The CT scanner is equipped with a microfocus x-ray tube by VISCOM (model XT 9225-DED), a flat panel detector by PerkinElmer (model XRD 1620 AN14), and a kinematic system by Carl Zeiss IMT. Table 1 summarizes the subsystems' characteristics. Regarding the positioning errors of the CT instrument, which are software-corrected, Müller [7] experimentally demonstrated that the kinematic system ensures a positioning of the test object down to the micrometer range. This way, inaccuracies of the kinematic system of the CT instrument were not taken into account, i.e., they were regarded as having negligible error in this work. The x-ray microfocus tube and the flat panel detector were modeled in the simulation environment with the information provided in Table 1 using respectively the software tools 'spectrum calculator' and 'detector calculator'. The source-to-detector distance was set to 1500 mm. The virtual model of the test object was then loaded and coarsely positioned between the x-ray source and detector.

2.3 Design of the virtual experimentation

The settings under the control of the CT metrologist were tuned observing good metrology practices and correlated with those considered during the real measurements of the test object. The virtual model of the test object was aligned in such a way that the distances to be traveled by x-rays and the variation of penetration depth during object rotation were minimized, and that the surfaces to be scanned were inclined at least 10° to the rotation axis. The virtual model was then finely positioned along the magnification axis to project it using the detector's maximum possible area, the tube voltage set high enough to avoid complete beam absorption (no pre-filter included), the detector integration time adjusted to a convenient value, the tube current tuned to enhance image contrast and brightness, and the number of projections chosen as approximately the number of pixels covered by the object's shadow in the projection. The object orientation and position (which defines the geometric magnification) and the tube voltage remained fixed during the measuring runs; the tube voltage, in fact, was adjusted when switching to the monochromatic spectrum to approximately the mean energy of the polychromatic spectrum. The other factors, i.e. (x-ray tube) current, focal spot size; (detector) integration time, unsharpness, noise factor, image averaging - were modified accordingly in order to explore their influence on the measurements.

Table 1: Technical specifications of the CT instrument subsystems, according to the manufacturers' datasheets.

component	parameter	value / attribute / type
x-ray tube	type	VISCOM XT 9225-DED
	acceleration voltage	(30 to 225) kV
	filament current	(10 to 3000) µA
	radiation production	reflection emitter
	target power	320 W (maximum)
	target material	tungsten | 1.0 mm thick
	reflected beam angle	50° (conical)
	intrinsic filtering	aluminum | 0.3 mm thick
flat panel detector	type	PERKINELMER XRD 1620 AN14
	total area / pixel matrix	(409.6 x 409.6) mm | 2048 x 2048 @ 200 µm
	radiation energy	40 keV to 15 MeV
	scintillator material	Gd_2O_2S:Tb | 208 µm thick
	ADC resolution	16 bits | 65536 gray levels
positioning system	type	Carl Zeiss IMT
	source-to-detector distance	1500 mm
	linear positioning system	three-axis kinematics | CAA (software) correction

For the sensitivity analyses, the following influence factors/parameters were taken into consideration: (x-ray tube) focal spot size and spectrum; (detector) unsharpness and noise; (interaction of x-ray and matter) beam hardening. The x-ray spectrum can be alternated between monochromatic and polychromatic; this allows us to visualize and quantify the effect of beam hardening artifacts on the measured quantities. The focal spot size can be defined either as an 'infinitesimal point' or as a 'regular grid of point sources' arranged over a rectangular zone; this allows us to observe the influence of the spot size on the measurements. Detector unsharpness (inherent blurring) can be simulated (by Gaussian filtering) and noise can be added (by setting a factor) to the synthetic image; this allows us to evaluate respectively the effect of varying the effective pixel size (e.g., using the function 'pixel binning' available in most detectors) and the detector sensitivity (gain). Further object-specific details on the virtual measurement setup are provided in the next section.

3 Virtual sensitivity analysis findings

Table 2 lists the parameters used for the 'realistic setup' (that mirrors the real experimental setup) and the parameters that were varied in the simulation environment. The detector multisampling option available in the simulator, used for anti-aliasing, was set as a regular grid with pattern 3x3. Before each simulation run, flat-field correction (available in the simulator) was applied to remove the shading in the image due to the different path lengths of the x-ray cone beam. The simulated radiographs were processed using the reconstruction module included in the simulator, which utilizes the conventional Feldkamp method. With this measurement scene, the simulation time was of the order of 90 min; it can be reduced by lowering the mesh accuracy of the virtual model of the test object. As for the surface determination from the reconstructed volume, the standard 'iso-50%' threshold value was applied globally (a reasonable choice since the test object is made of a single homogeneous material) later on within VG Studio MAX, version 3.3.2 64 bit. To evaluate the dimensional quantities of the test object in all measurement scenarios, a best-fit registration of the reconstructed volume against the CAD model was performed first in order to define a common local coordinate system; then, a measurement template (containing the reference objects and associated features of interest), which was previously created using as reference the mathematical model, was imported and the measurement results automatically calculated (least-squares method used to fit the points to the ideal feature).

3.1 Influence of detector unsharpness

The detector image unsharpness is one of the settings that can be overridden in the simulation software by Gaussian filtering. The default inherent unsharpness of the detector was set to twice the basic spatial resolution (i.e., effective pixel size, assumed to be 0.04 mm). By entering different values for the inherent unsharpness of the detector and different basic spatial resolution, the CT metrologist can evaluate the influence of changing the number of image points, e.g., by setting the binning mode of the detector. In principle, by assigning an unsharpness value smaller than the one originally attributed to the detector, more data is to be sensed by the detector; contrarily, by assigning an unsharpness value larger than that originally attributed to the detector, less data is to be captured by the detector. The effect of different inherent unsharpness of the detector was investigated in four setups for the monochromatic spectrum: (s0: 2xBSr) unsharpness of 0.08 mm (default), (s1: 1xBSr) unsharpness of 0.04 mm, (s2: 3xBSr) unsharpness of 0.12 mm, (s3: 4xBSr) unsharpness of 0.16 mm; and in three setups for the polychromatic spectrum: (s0': 2xBSr) unsharpness of 0.08 mm (default), (s1': 1xBSr) unsharpness of 0.04 mm, (s2': 3xBSr) unsharpness of 0.12 mm.

Table 2: CT parameters used for the 'realistic setup' and the 'alternative setups' in the virtual measurement scene.

component	parameter	realistic setup	alternative setups
x-ray source	energy spectrum	polychromatic	polychromatic / monochromatic
	acceleration voltage	120.0 kV	45.0 kV (for monochromatic)
	filament current	225.0 µA	337.5 µA / 450.0 µA
	pre-filter thickness	none	none
	focal spot (type) size	(point)	(3x3) 60 µm / 90 µm / 120 µm
flat panel detector	no. of pixels (H/V)	1024	512 / 768 / 2048
	integration time	1 s	0.5 s / 0.75 s
	no. of frames to average	1	4
	unsharpness	0.8 mm	0.4 mm / 1.2 mm / 1.6 mm
	noise factor	1x	5x / 10x / 20x
test object setup	distance source-detector	1500.0 mm	1500.0 mm
	distance source-object	250.0 mm	250.0 mm
	geometric magnification	6.0x	6.0x
	rotation about x-axis	0°	0°
	rotation about y-axis	20°	20°
	rotation about z-axis	-110°	-110°
	no. of projections	720	720

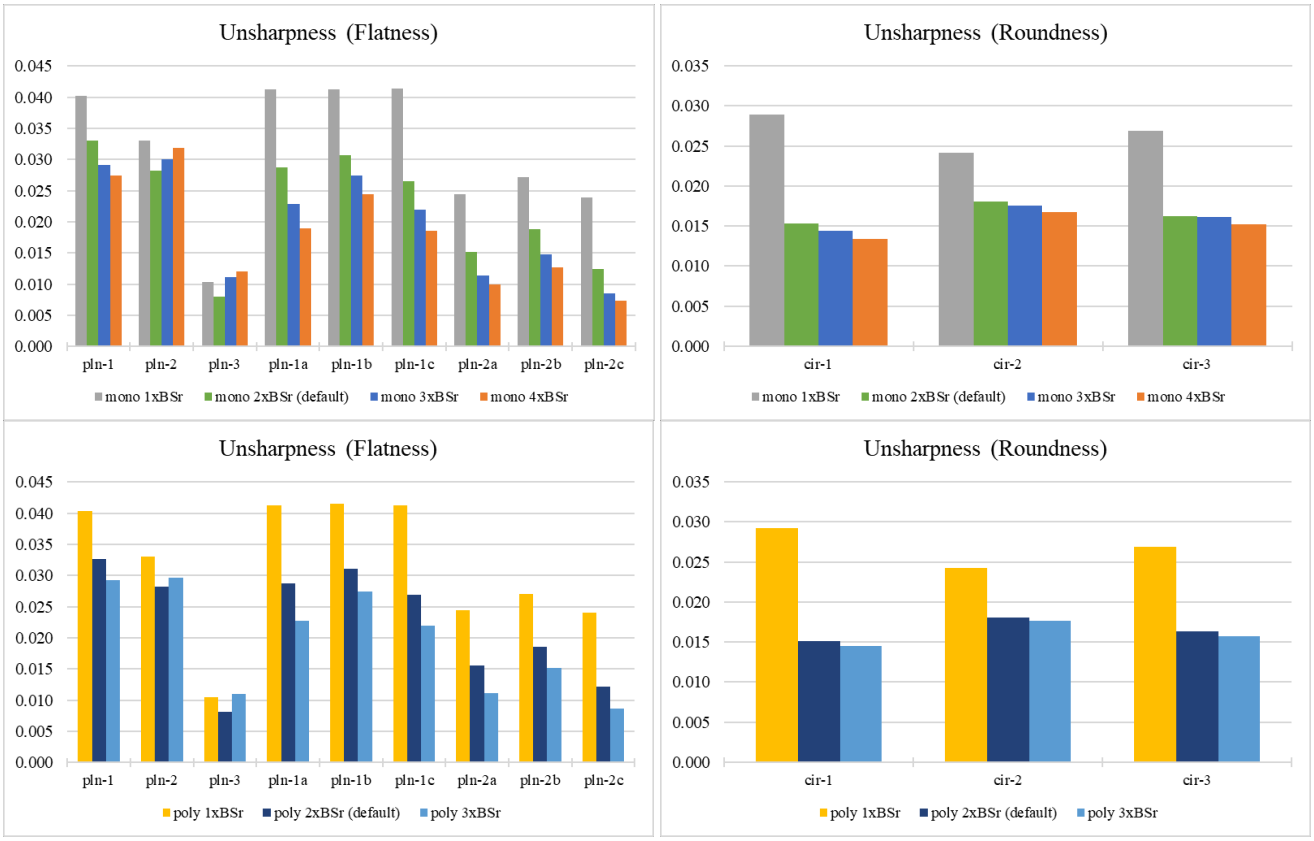

Figure 2: Graphs showing the influence of changing the inherent unsharpness on the form of planes (left) and circles (right) of the test object. Upper graphs show the results for the monochromatic spectrum; lower graphs, for the polychromatic spectrum. Values in millimeters.

Figure 2 shows the form error values calculated for the planes (left) and the circular sections (right) using the monochromatic spectrum (top) and polychromatic spectrum (bottom) in each setup. As expected, the larger the inherent unsharpness value, the lower the form error value. This effect is explained by the filtering imposed by the limited structural resolution associated with CT images (radiographs and reconstructed volume) containing less information (blurred images), in which smaller structures can no longer be resolved (and consequently measured). Absolutely no difference in the variation pattern could be observed when comparing the form error values for the monochromatic and polychromatic spectra. It is worthy of notice that the object projections were generated from a mesh file created using the nominal model of the object; therefore, the form error (variation) observed for the features is on the one hand related to the CT measurement setup under scrutiny, and on the other hand linked to

limitations of the virtual setup, such as insufficient number of point sources for focal spot simulation, insufficient detector multisampling (which give rise to signal aliasing); they can be fixed by increasing the corresponding input parameters at the cost of (prohibitive) simulation time.

Regarding the intrinsic characteristics (circle diameter) and the situation characteristics (distance between planes), the results are displayed on the graphs in Figure 3. For both dimensional characteristics investigated, the larger the unsharpness, the more the results depart from the reference (zero) line. This means that the lack of information associated with blurred images not only reduces the capability of CT to resolve form deviation on the test object, but also decreases the measurement accuracy for dimensional quantities. For outer sizes, the departure from the reference line is much more evident than that observed for inner sizes. For the distances between planes, the detrimental effect of increasing the detector unsharpness is clearly visible, particularly for bidirectional distances (e.g., distance between pln-1 and pln-2, distance between pln-1 and pln-3). In the worst case, the observed error was close to 0.04 mm. As for the radiation spectrum, in general, the deviation from the nominal value observed for the polychromatic spectrum was slightly less than that observed for the monochromatic spectrum, in consonance with the results reported by Helmecke et al. [8], even though the reason for that is, in fact, unknown.

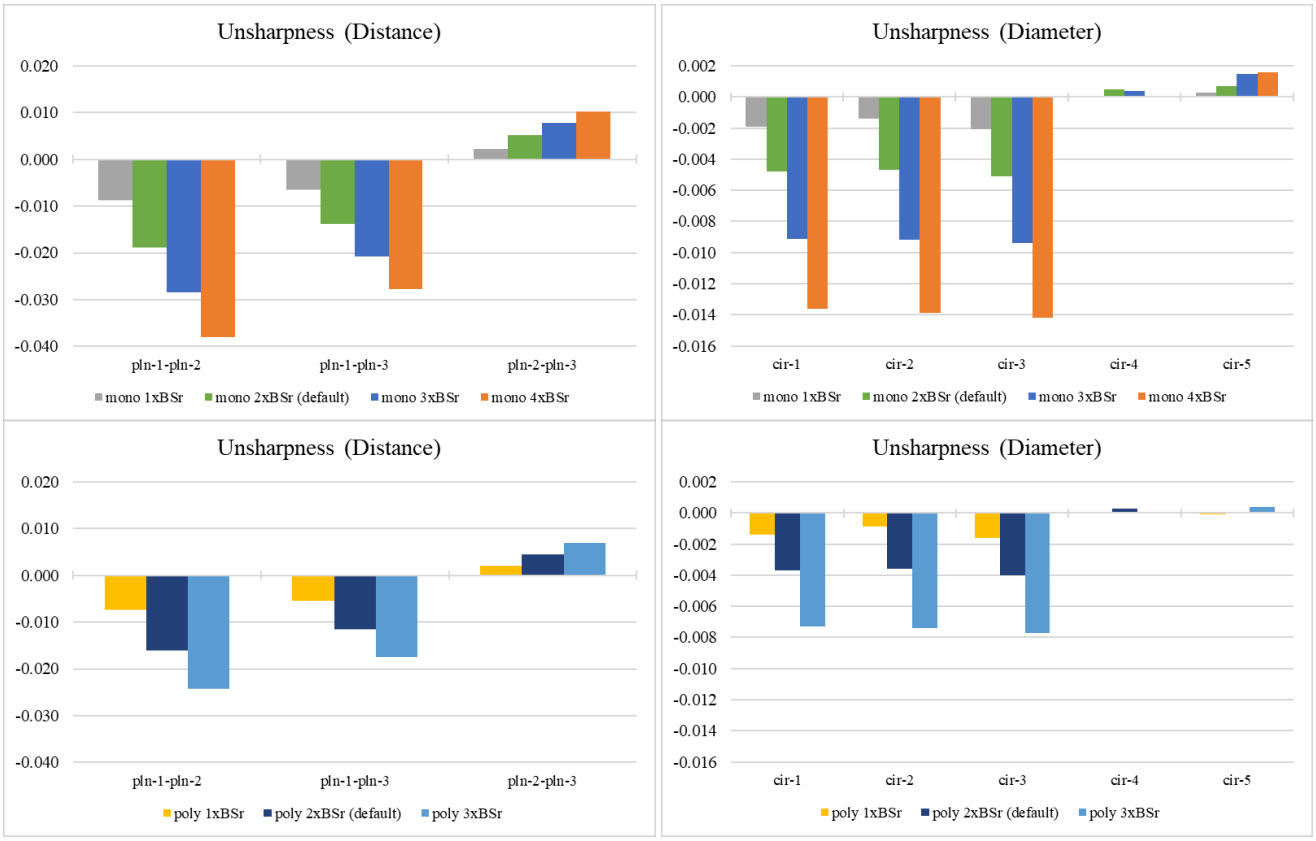

Figure 3: Graphs showing the influence of changing the inherent unsharpness on distances (left) and diameters (right) of the test object. Upper graphs show the results for the monochromatic spectrum; lower graphs, for the polychromatic spectrum. Values in millimeters.

3.2 Influence of detector noise and image averaging

In the simulation environment, quantum noise and electronic noise can be added to the image pixel by pixel depending on its grey value by assigning a single noise factor. In practice, favorable signal intensity can be achieved by increasing the filament current and integration time, as well as by averaging an appropriate number of images in each rotary position, as more photons can be absorbed by the detector. The signal-to-noise ratio can be improved this way; albeit the CT metrologist needs to bear in mind that by increasing the filament current, the focal spot becomes larger as well. The product of current and integration time was kept constant during the virtual experiments; otherwise, the contrast between the object and the background during image acquisition would not be satisfactory. The effect of changing the current and integration time is presented in section 3.3, when evaluating the variable ‘focal spot size’. The image signal can be made stronger or weaker by adjusting the photodiodes’ gain factor, which changes the sensitivity of the detector. By increasing the gain, the image signal becomes stronger (brighter) and, proportionally, the image blurring increases (becomes noisier); in this regard, image averaging can be employed to reduce noise in the projections. The effect of varying these two parameters was examined in the simulation environment considering five setups using the monochromatic spectrum: (s0) noise factor = 1x (default), (s1) noise factor = 5x, (s2) noise factor = 10x, (s3) noise factor = 20x, (s4) noise factor = 20x and number of frames to average = 4.

Figure 4 shows the form error values obtained for the planes (left) and the circles (right) in each setup. By increasing the noise factor, the form error increases in an upward trend in most cases; more evident when small planes (pln-3, flatness for the whole surface; pln-1a, pln-1b, pln-1c, pln-2a, pln-2b, pln-2c, i.e., flatness on a unit basis) and circles were considered. For setup (s4), the results converged in most cases to those observed for setup (s2), as expected. Therefore, whenever the signal-to-noise ratio needs to be improved and the focal spot size imposes limits to a higher current, the image averaging should be kept in view. Figure 5 exhibits the results for the situation characteristics (distance between planes) and the intrinsic characteristics (circle diameter) for each measurement case. For the diameters, it is clear that the measurement bias departs more from the reference (zero) line as the noise factor increases. The effect is similar for both outer and inner diameters, even though the absolute error is remarkably larger for outer sizes. The reason for this significant difference requires further investigation, especially because at this point a monochromatic spectrum was used. On the other hand, for the distances between planes, the influence of increasing the detector noise is nearly imperceptible. For the distance between pln-2 and pln-3, which is not affected by edge detection, the absolute error is significantly smaller than those observed for the other two distances; for the distance between pln-1 and pln-2 (nominal value of 2 mm), the observed error was close to 0.02 mm.

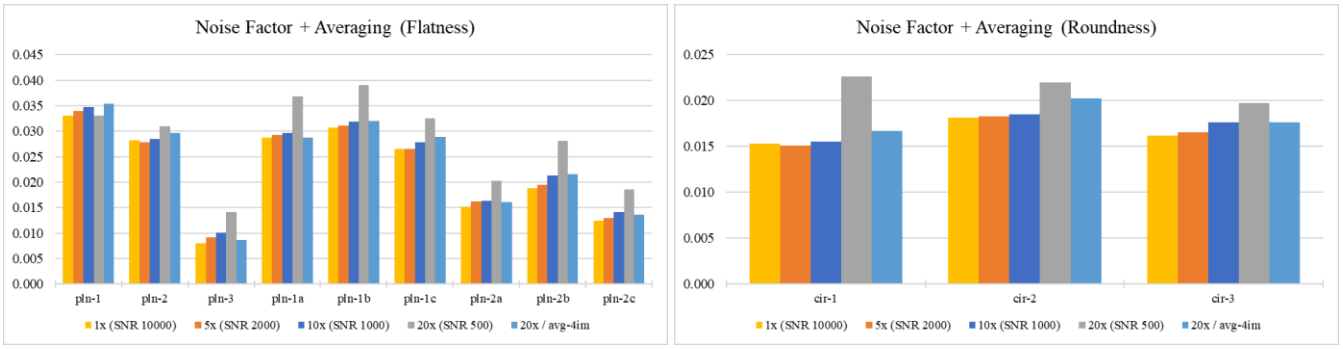

Figure 4: Column graphs showing the effect of varying the noise factor and image averaging on the form of planes (left) and circles (right). Measured values displayed in millimeters,

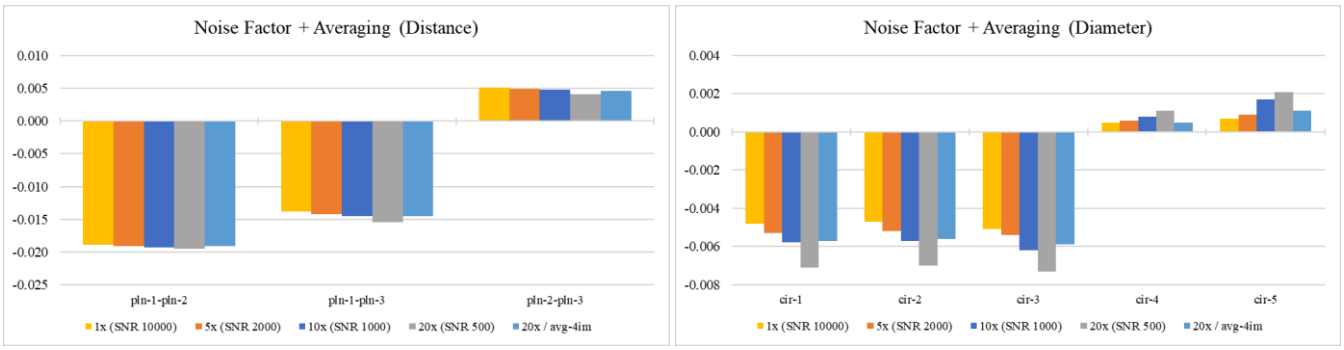

Figure 5: Column graphs showing the effect of varying the noise factor and image averaging on distances (left) and diameters (right). Measured values displayed in millimeters,

3.3 Influence of focal spot size

In addition to the inherent unsharpness of the detector, the geometric unsharpness of the image can be also affected by the size of the focal spot. The effect of increasing the focal spot size on the dimensional quantities of the test object was investigated in three conditions for the monochromatic spectrum: (s0) punctiform source, (s1) spot size = 60 µm, (s3) spot size = 120 µm; and four conditions for the polychromatic spectrum: (s0') punctiform source, (s1') spot size = 60 µm, (s2') spot size = 90 µm, (s3') spot size = 120 µm. To give an approximate estimate of the focal spot size, one relied on the empirical linear relations derived by Hiller et al. [9]. The practical guidance that the focal spot size should not be greater than the voxel size was satisfied for the smallest focal spot size only (60 µm); for the two other setups, the geometric unsharpness might have a detrimental impact on the image quality (and on the measurement results). However, as can be seen in Figure 6, the increase of tube power (and spot size) did not have a significant effect on the form of the dimensional features, except for the polychromatic spectrum with a focal spot size of 120 µm, approximately twice the voxel size. For some reason, unknown to this point, but probably associated with some inaccuracy of the simulation environment, this strong filtering behavior was not replicated by the monochromatic spectrum. In addition, the slight (upward) trend verified for the polychromatic spectrum would not be the expected response to the increase of the focal spot size. As for the distances between planes and sizes, the variation pattern seems to be random for the monochromatic spectrum (upper graphs shown in Figure 7). For the polychromatic spectrum, a linear trend can be noticed in most cases (except the inner diameters); the departure from the reference (zero) line decreases with the increase of the focal spot size. This finding opposes that observed for the detector inherent unsharpness, illustrated in Figure 3.

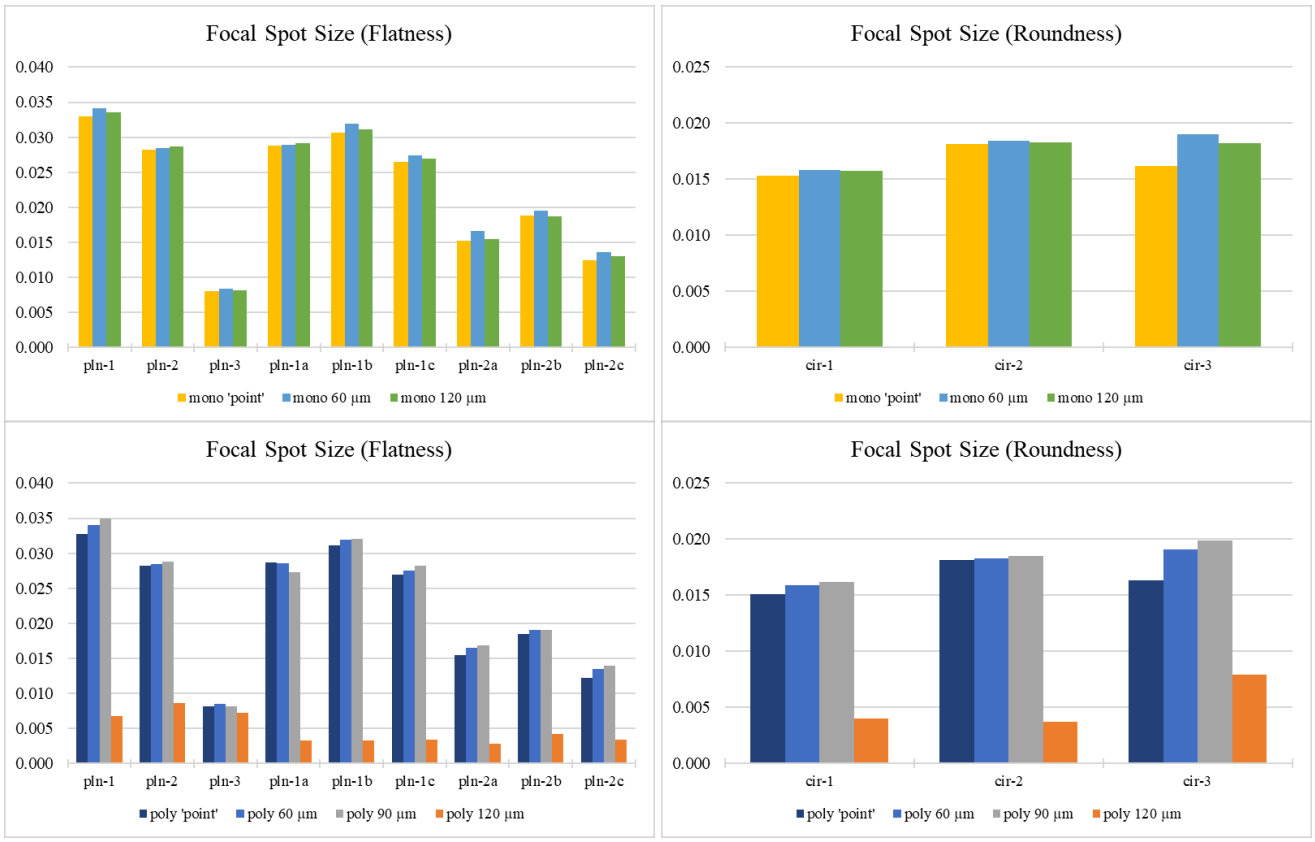

Figure 6: Column graphs showing the influence of changing the focal spot size on the form of planes (left) and circles (right). Upper graphs show the results for the monochromatic spectrum; lower charts, the results for the polychromatic spectrum. Values in millimeters.

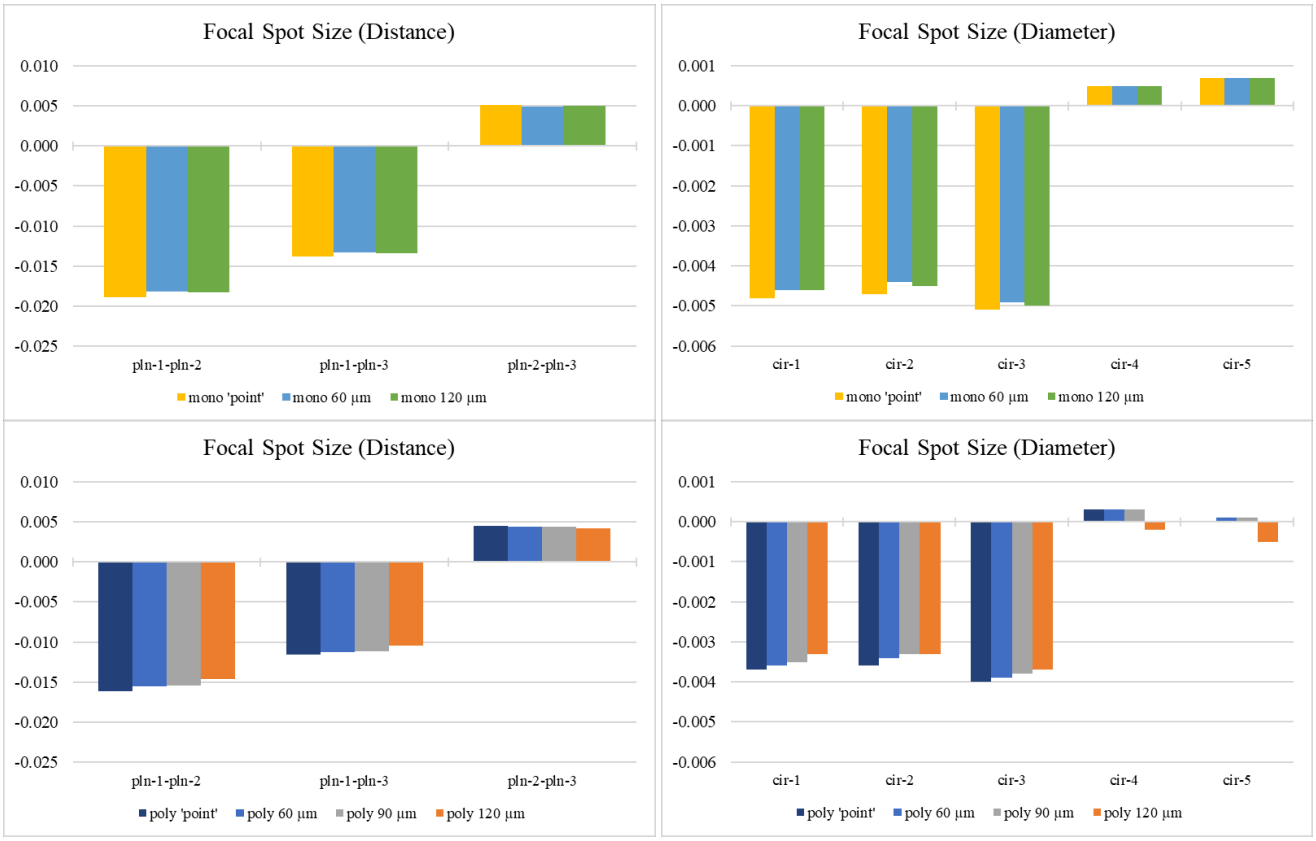

Figure 7: Column graphs showing the effect of changing the focal spot size on distances (left) and diameters (right). Upper graphs show the results for the monochromatic spectrum; lower graphs, the results for the polychromatic spectrum. Values in millimeters.

3.4 Influence of radiation spectrum (and interaction with matter)

The radiation spectrum generated in an x-ray tube of CT instruments used for dimensional measurements is not monoenergetic, in which the absorption curve is a straight line on the logarithmic scale. Indeed, it is a continuous radiation spectrum with a specific bandwidth, which is overlaid by a line spectrum depending on the tube voltage and target material. The parts of the radiation spectrum with less energy are more easily attenuated by matter than those with high energy. This phenomenon is responsible for beam hardening artifacts. Beam hardening is one of the significant artifacts in CT images that come from a polychromatic nature of x-ray energy, which leads to an error in attenuation coefficient in which the basic assumption to represent the attenuation in CT is a monochromatic beam, where attenuation does not change with energy spectrum [10]. To investigate the influence of the radiation spectrum on the measurement of the dimensional quantities, one first executed the simulation for the 'realistic setup' listed in Table 2, and later one carried out another simulation run, but switching the radiation spectrum to monochromatic and adjusting the voltage accordingly. The results for the form errors, displayed in Figure 8 (upper graphs), were nearly identical regardless of the type of radiation spectrum used. For the distances and diameters, the results for the monochromatic spectrum departed more from the reference line than the ones for the polychromatic spectrum, as can be seen in Figure 8 (lower graphs). These findings are in line with the results reported by Helmecke et al. [8]. From another view, assuming the values obtained with the monochromatic spectrum as reference, the use of the polychromatic spectrum resulted in a measurement bias with a pattern that resembles that observed in an experimental work previously carried out using modular test pieces [11–12]. The absolute value of these biases was of the order of 0.001 mm for the outer diameters, less than 0.001 mm for the inner diameters, and less than 0.003 mm for the distances between planes; especially for the circle diameters, the simulated biases were not even close to the ones observed in real experiments with the same test object on the CT instrument mirrored in the simulation software. Using a measurement setup similar to the one replicated in simulation, the measurement bias observed for the real experiments was approx. 20 times greater than that obtained from simulation, as can be seen in [6].

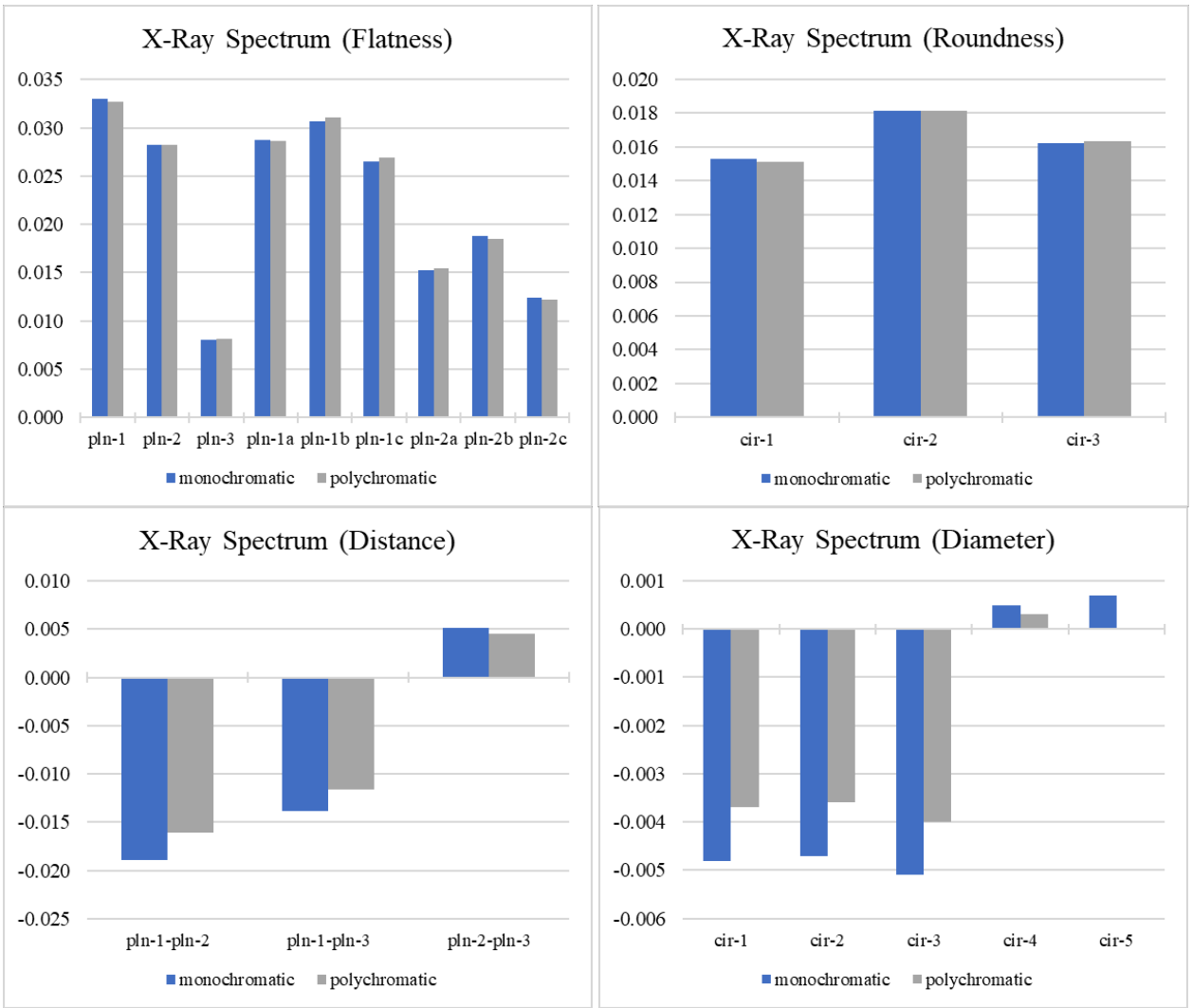

Figure 8: Column graphs showing the differences observed for the dimensional parameters of the test object when switching from a monochromatic spectrum to a polychromatic spectrum. Measured values displayed in millimeters.

4 Concluding remarks

The creation of a digital twin of the CT instrument Carl Zeiss IMT METROTOM 1500 and the main findings of the virtual experiments performed with a plastic part were presented in this paper. Some of the results confirmed one's theoretical and empirical background. For the inner unsharpness and noise of the detector, simulated respectively by Gaussian filtering and by adding noise to the image pixel by pixel depending on its grey value, in general, the results were just as expected: (a) the larger the inherent unsharpness value, the lower the form error value, (b) the larger the inherent unsharpness value, the larger the error for sizes and distances, (c) the higher the noise factor, the larger the form error value, (d) the higher the noise factor, the larger the error for sizes (for distances, no difference could be detected). In opposition to these expected outcomes, the increase of the focal spot size did not have a significant effect on the form of the dimensional features. As for the distances between planes and circle diameters, an unexpected random pattern was verified with the monochromatic spectrum and an upward linear trend could be noticed with the polychromatic spectrum, which differs from the downward linear trend observed for the detector inherent unsharpness. Based on the findings described here, questions could be raised about the accuracy of the measurement model to predict the systematic components of the measurement error, particularly those stemming from the interaction of x-ray and matter. For this reason, other analyses will be conducted on the simulation platform considering, e.g., other materials and geometries; additionally, the integrity of the measurement model relating the output quantity and the input quantities will be further investigated.

Acknowledgements

The first author wishes to express his thanks for the financial support of São Paulo Research Foundation (FAPESP), grant #2018/24757–7, within the Research Fellowships Abroad (BPE) program.

References

[1] J-P. Kruth, A. Weckenmann, S. Carmignato, R. Schmitt, M. Bartscher, L. De Chiffre, Computed tomography for dimensional metrology, CIRP Ann.—Manuf. Technol. 60 (2011) 821–842.

[2] S. Reisinger, S. Kasperl, M. Franz, J. Hiller, U Schmid, Simulation-based planning of optimal conditions for industrial computed tomography, e-J. Nondestr. Test. 16(11) (2011) 1–8.

[3] J. Hiller, L.M. Reindl, A computer simulation platform for estimation of measurement uncertainties in dimensional x-ray computed tomography, Measurement 45 (2012) 2166–2182.

[4] E. Helmecke, M. Fleßner, M. Kaufmann, A. Staude, T. Hausotte, Numerical measurement uncertainty determination for dimensional measurements of microparts with CT, e-J. Nondestr. Test. 21(2) (2016) 1–7.

[5] F. Wohlgemuth, T. Hausotte, Convergence behaviour of numerical measurement uncertainty evaluation using a virtual metrological computed tomography system, e-J. Nondestr. Test. 25(2) (2019) 1–10.

[6] T.L. Fernandes, C.R. Baldo, G.D. Donatelli, Experimental evaluation of the uncertainty associated with the result of feature-of-size measurements through computed tomography, J. Phys.: Conf. Ser. 733 (2016) 012056.

[7] P. Müller, Coordinate metrology by traceable computed tomography, PhD Thesis, Technical University of Denmark (2013) Copenhagen, Denmark.

[8] E. Helmecke, M. Fleßner, A. Gröschl, A. Staude, T. Hausotte, Numerical measurement uncertainty determination for computed tomography in dimensional metrology, IMEKO World Congress (2015) Prague, Czech Republic.

[9] J. Hiller, M. Maisl, L.M. Reindl, Physical characterization and performance evaluation of an x-ray micro-computed tomography system for dimensional metrology applications, Meas. Sci. Technol. 23 (2012) 085404.

[10] O.M.H. Ahmed, Y. Song, A review of common beam hardening correction methods for industrial x-ray computed tomography, Sains Malaysiana 47 (2018) 1883–1890.

[11] C.R. Baldo, T.L. Fernandes, G.D. Donatelli, Experimental investigation of computed tomography dimensional capability using modular test artefacts IMEKO World Congress (2015) Prague, Czech Republic.

[12] C.R. Baldo, T.L. Fernandes, G.D. Donatelli, Experimental assessment of computed tomography dimensional performance using modular test pieces made of polyoxymethylene and aluminum, e-J. Nondestr. Test. 21(2) (2016) 1–7.